SYNTHESIS AND SINTERING 6 (2026) 49–56

Available online at www.synsint.com

Synthesis and Sintering

ISSN 2564-0186 (Print), **ISSN** 2564-0194 (Online)

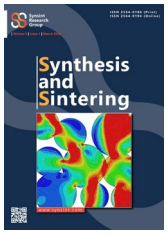

Perspective

The expanding role of the Anstis relationship in advanced materials research: A perspective

Maryam Mohammadpour Mokhayer [a,b,*], **Mahdiyeh Omrani Khiabanian** [b]

[a] *Department of Industrial Engineering, University of Trento, Trento, Italy*
[b] *Department of Mechanical Engineering, University of Tabriz, Tabriz, Iran*

A B S T R A C T

Fracture toughness remains one of the most important parameters governing the structural reliability of brittle and quasi-brittle materials. Across a broad-spectrum of 2026 studies, the Anstis relationship continued to serve as one of the most widely adopted methods for evaluating indentation fracture toughness in ceramics, glass-ceramics, thermal barrier coatings, solid electrolytes, high-entropy systems, carbides, borides, composites, geological materials, and additively manufactured structures. The reviewed studies collectively demonstrate that the Anstis relationship remains valuable because it enables fracture toughness estimation from indentation-derived crack lengths while maintaining experimental simplicity and compatibility with heterogeneous or miniature materials systems. The collected publications further reveal a growing integration of fracture toughness evaluation with advanced microstructural engineering strategies including additive manufacturing, spark plasma sintering, eutectic architecture design, high-entropy alloying, defect engineering, phase transformation, residual stress tailoring, and interface-controlled reinforcement. Toughening mechanisms repeatedly observed across the literature include crack deflection, crack bridging, grain refinement, residual compressive stress development, transformation toughening, grain boundary pinning, and multiphase reinforcement. Applications span aerospace systems, thermal/environmental barrier coatings, dental restorations, hydrogen storage alloys, transparent ceramics, radiation shielding glasses, all-solid-state batteries, and ultra-high-temperature structural ceramics. The present perspective integrates fragmented findings from the 2026 excerpts provided into a coherent overview of the expanding role of the Anstis relationship in contemporary materials science research.

KEYWORDS

Anstis relationship
Indentation fracture toughness
Brittle materials
Toughening mechanisms
Advanced ceramics

OPEN ACCESS

1. Introduction

Fracture toughness is a critical parameter for evaluating the mechanical reliability and structural integrity of brittle and semi-brittle materials, particularly ceramics, carbides, oxides, glass-ceramics, coatings, and advanced functional systems. In these materials, crack initiation and propagation dominate failure behavior, making fracture resistance essential for long-term performance and operational safety. Consequently, accurate fracture toughness characterization remains a major focus in modern materials science research [1].

Among available characterization approaches, indentation-based fracture mechanics has become particularly attractive because of its experimental simplicity and applicability to small-scale, heterogeneous, or difficult-to-machine materials. In this context, the Anstis relationship has emerged as one of the most widely employed methods for estimating fracture toughness from

* Corresponding author. *E-mail address:* m.mohammadpour@unitn.it (M. Mohammadpour Mokhayer)
Received 22 July 2025; Received in revised form 30 March 2026; Accepted 30 March 2026.

https://doi.org/10.53063/synsint.2026.61302

indentation-induced cracks [1]. The reviewed studies consistently demonstrate that the relationship enables evaluation of fracture resistance using measurable parameters such as indentation load, crack length, hardness, and elastic modulus. The collected 2026 publications repeatedly employed the Anstis relationship for fracture toughness determination in brittle materials.

The Anstis relationship for fracture toughness is given in Eq. 1:

$$K_{IC} = 0.016\left(\frac{E}{H_v}\right)^{1/2}\left(\frac{P}{C^{3/2}}\right) \quad (1)$$

where H_v is the Vickers hardness, E is Young's modulus, P is the indentation load, and C is half of the radial crack length.

To better understand the mechanical principles underlying these formulations, the geometric configuration of the indentation process and the corresponding stress fields are schematically illustrated in Fig. 1. The diagram highlights how the application of a sharp Vickers indenter with load *P* induces a localized plastic zone, from which radial "half-penny" cracks propagate outward to a length c from the center of an impression with a half-diagonal a. As demonstrated in the 2026 literature, the precise determination of the crack-to-indent ratio is paramount, as it dictates whether the standard Anstis calibration factor (0.016) or modified formulations incorporating Vickers hardness (H_v) are strictly applicable for a given brittle or quasi-brittle matrix.

The reviewed studies collectively emphasized that the Anstis relationship is particularly advantageous because it avoids the need for complex specimen geometries and extensive sample preparation. The method therefore remains highly suitable for ceramics, coatings, glass systems, geological materials, solid electrolytes, carbides, borides, and high-entropy systems.

Several studies additionally highlighted methodological considerations governing accurate indentation fracture analysis. In brittle oxide ceramics, the ratio between indentation size and crack length (l/α) was identified as an important factor for selecting appropriate fracture calculations, while radial and half-penny crack models were repeatedly used for interpreting indentation behavior [2]. Nanoindentation and Vickers indentation methods were frequently combined with hardness and elastic modulus measurements to establish integrated structure–property relationships [3].

Beyond conventional indentation analysis, complementary computational methodologies were also introduced. A MATLAB-based framework incorporating path-independent J- and M-integrals enabled the extraction of stress intensity factors directly from experimental displacement fields, providing geometry-independent characterization of defects under small-strain conditions [4].

The collected studies further demonstrate that the Anstis relationship is no longer applied merely as a routine characterization method. Instead, fracture toughness evaluation has become integrated with advanced materials design strategies involving additive manufacturing, spark plasma sintering, high-entropy alloy development, thermal barrier coatings, interface engineering, and multifunctional optimization.

2. Fracture toughness evaluation in advanced ceramics

2.1. Ultra-high-temperature ceramics

Ultra-high-temperature ceramics (UHTCs) represented one of the most important application areas for indentation fracture toughness analysis in 2026 research. These materials require exceptional resistance to crack propagation under severe thermal and mechanical loading conditions.

A notable investigation examined TiB_2, ZrB_2, and ZrC components fabricated through direct ink writing combined with pressureless spark plasma sintering. TiB_2 exhibited superior overall performance, achieving hardness values of 26 ± 1 GPa together with indentation toughness values of 7 ± 1 MPa.m$^{1/2}$. The study emphasized the importance of controlling drying and printing conditions to suppress crack formation during processing [5].

Additively manufactured zirconium carbide fabricated through material extrusion and pressureless sintering achieved relative densities of 90.3% with fracture toughness values of 2.9 ± 0.2 MPa.m$^{1/2}$. Griffith analysis identified large grains as dominant fracture-controlling flaws [6].

Ti_2AlC reinforced ZrB_2 systems demonstrated substantial improvements in densification and fracture resistance. Relative density increased from 80% in monolithic ZrB_2 to 98% in reinforced composites, while fracture toughness increased from 2.0 to 5.3 MPa.m$^{1/2}$. Crack bridging, crack deflection, and strengthened grain boundaries contributed significantly to the observed toughening behavior [7].

Tantalum boride ceramics also exhibited improved mechanical performance following Si_3N_4 addition, reaching fracture toughness values of 4.40 MPa.m$^{1/2}$ [8]. Similarly, lanthanum hexaboride systems reinforced with Ni displayed nearly doubled fracture toughness owing to crack bridging and crack deflection mechanisms [9].

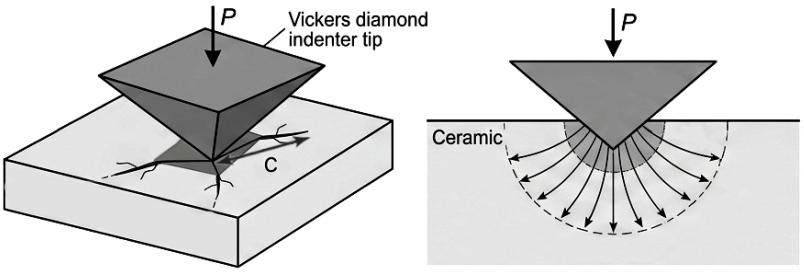

Fig. 1. Anstis indentation schematics.

2.2. Oxide ceramics and mullite systems

Oxide ceramics remained one of the most extensively investigated material classes using the Anstis relationship.

RE_3TaO_7 ceramics exhibited hardness values ranging from 5.8 to 14.9 GPa and elastic modulus values between 127.5 and 247.8 GPa, while fracture toughness remained within 1.0–2.0 MPa.m$^{1/2}$. These characteristics supported their applicability in thermal barrier coating systems [2]. Hafnia ceramics processed under high pressure achieved fracture toughness values near 3.00 MPa.m$^{1/2}$ together with improved density and grain refinement [10].

Mullite ceramics synthesized through arc plasma processing demonstrated strong dependence of fracture toughness on powder particle size distribution and microstructural homogeneity. The resulting materials achieved densities of 2.85 g/cm^3, microhardness values near 10.8 GPa, and fracture toughness values around 2.9 MPa.m$^{1/2}$ [11].

Advanced alumina systems exhibited multiple toughening strategies. Al_2O_3/ZrO_2 eutectic systems achieved fracture toughness values approaching 9.8 MPa.m$^{1/2}$ through optimized yttria concentration and eutectic microstructures [12]. TiO_2-modified zirconia-toughened alumina achieved fracture toughness values of 6.08 MPa.m$^{1/2}$ owing to enhanced densification and microstructural refinement [13]. Nano-zirconia reinforced alumina composites further demonstrated improvements through crack deflection, transformation toughening, and grain boundary pinning [14].

3. Carbides and high-entropy systems

The fully dense $(TiZrNbTa)C_{0.8}N_{0.2}$ high-entropy carbonitride synthesized under high-pressure and high-temperature conditions exhibited hardness values of 19.6 GPa and fracture toughness values of 5.6 MPa.m$^{1/2}$. In situ synchrotron diffraction confirmed structural stability up to 28.7 GPa [15].

Nonstoichiometric high-entropy (TaNbZrTiMo)C ceramics demonstrated strong sensitivity of toughness behavior to carbon content. Hardness and fracture toughness initially increased with carbon concentration before decreasing at higher contents. Maximum fracture toughness values reached 3.84 ± 0.32 MPa.m$^{1/2}$ [16]. High-entropy hydrogen storage alloys based on Ti–Zr–V–Cr–(Co,Fe) were evaluated using the Anstis relationship to investigate crack resistance under hydrogen exposure. The work emphasized the importance of fracture toughness in mitigating hydrogen-induced embrittlement [17].

Carbide systems also received extensive attention. TiCrC nanocarbides achieved fracture toughness values of 6.5 MPa.m$^{1/2}$ alongside high hardness and compressive strength [18]. In (V,Nb)C carbides, spinodal decomposition generated nanoscale phase separation that simultaneously improved hardness and fracture toughness by approximately 25% [19].

Silicon carbide-based multiphase systems additionally exhibited enhanced fracture resistance through AlN and VC additions. Solid solution formation and grain boundary pinning increased fracture toughness up to 5.25 MPa.m$^{1/2}$ [20].

Mechanically activated Ti_3AlC_2 MAX phase systems formed $Al_2O_3/TiC_x/Ti_3AlC_2$ nanocomposites following heat treatment [21]. The resulting materials retained fracture toughness values of 7.6 MPa.m$^{1/2}$ while exhibiting hardness near 13 GPa.

4. Thermal barrier coatings and functional ceramics

Thermal barrier coatings (TBCs) and environmental barrier coatings (EBCs) represented another major application area for indentation fracture analysis.

$Hf_6Ta_2O_{17}$/YSZ (yttria-stabilized zirconia) dual-ceramic coatings exhibited superior $CaO–MgO–Al_2O_3–SiO_2$ (CMAS) corrosion resistance and oxidation stability compared with conventional YSZ coatings. The coatings survived 1496 thermal cycles at 1200 °C and showed a microhardness of 9.98 GPa and a fracture toughness of 3.01 MPa.m$^{1/2}$ [22]. $YbTaO_4$-Ta_2O_5 thermal environmental barrier coatings designed for SiC fiber/SiC composites achieved thermal cycling lifetimes exceeding 500 cycles at 1350 °C. Following corrosion testing, coated composites retained 73.91% of their strength, and their fracture toughness reached 3.52 MPa.m$^{1/2}$ [23]. $HfTiO_4$-TiO_2 composites optimized for thermal/environmental barrier applications demonstrated excellent compatibility with SiC-based systems while maintaining strong resistance to water-vapor corrosion and CMAS attack, and the Anstis relationship provides a reliable method to quantify their fracture toughness [24]. Pr_6O_{11}-doped ZrO_2 thermal barrier coatings additionally correlated fracture toughness directly with doping concentration and thermal stability [25].

Transparent ceramic systems revealed a different balance between optical and mechanical performance. SrF_2 transparent ceramics exhibited relatively low fracture toughness values of 0.31 MPa.m$^{1/2}$ despite improved optical transmittance achieved through grain growth strategies [26].

Transparent MgO-Al_2O_3-SiO_2-ZnO-B_2O_3 glass-ceramics achieved simultaneous improvements in hardness, fracture toughness, and visible transmittance [27]. Residual compressive stresses generated during crystallization contributed to crack deflection and interfacial strengthening.

5. Glass-ceramics, dental systems, and energy materials

5.1. Dental glass-ceramics

Dental materials represented one of the most prominent application areas for Anstis-based fracture toughness analysis.

Lithium disilicate glass-ceramics were extensively studied to correlate crystallization pathways with crack resistance [28]. Substitution of P_2O_5 with TiO_2 altered nucleation and grain growth behavior. P_2O_5 promoted homogeneous bulk nucleation, whereas TiO_2 promoted growth-dominated crystallization associated with enhanced fracture resistance [29]. Zirconia-containing lithium silicate glass-ceramics were additionally investigated through in situ nanoindentation inside scanning electron microscopy systems. Pre-crystallized materials displayed edge chipping and radial cracks, while crystallized structures exhibited shear-band formation and pile-up behavior [30].

Rotational cyclic contact wear studies further demonstrated strong relationships between microstructure, wear behavior, and crack propagation. Zirconia displayed the highest wear resistance among all tested systems [31].

5.2. Radiation shielding and functional glasses

Borotellurite glasses modified with Sb_2O_3 exhibited increasing fracture toughness with increasing additive concentration. Fracture toughness increased from 1.764 MPa.m$^{1/2}$ to 1.968 MPa.m$^{1/2}$ as Sb_2O_3

Table 1. Recurring toughening mechanisms reported in the literature.

Toughening mechanism	Representative systems	Reported effect
Crack deflection	Carbon fiber (C_f)/Si_3N_4, glass-ceramics, ZrB_2 composites	Increased crack path tortuosity
Crack bridging	Carbon-fiber systems, Ti_2AlC/ZrB_2	Enhanced energy dissipation
Residual compressive stress	Glass-ceramics, multiphase systems	Suppressed crack initiation
Grain refinement	High-entropy ceramics, lithium disilicates	Improved hardness and strength
Phase transformation	Zirconia-toughened alumina (ZTA) systems, Ti_3AlC_2-derived systems	Modified crack propagation
Grain boundary pinning	SiC–AlN–VC, zirconia-containing systems	Crack suppression
Interface engineering	G/carbon fiber reinforced alumina, metallic composites	Improved stress transfer
Porosity reduction	SPS-processed ceramics	Enhanced mechanical integrity

concentration increased. Gd_2O_3-modified borate glasses were similarly investigated for radiation shielding applications, where compositional modification influenced crack resistance and mechanical integrity [32]. CdZnTe crystals grown in hydrogen atmospheres exhibited enhanced fracture resistance owing to reduced defect density and improved lattice quality [33].

5.3. Solid electrolytes and energy systems

The reviewed publications demonstrated increasing use of the Anstis relationship in solid-state battery research and energy-related systems. Additional studies involving Li_2S:P_2S_5 glass, Li_3PS_4 glass ceramic, Li_6PS_5Cl, and $Li_{6.25}Ga_{0.25}La_3Zr_2O_{12}$ demonstrated that densification through molding pressure and sintering temperature improved both ionic transport and mechanical integrity [34].

These studies collectively demonstrate that fracture toughness evaluation is becoming increasingly important for ensuring the reliability and safety of all-solid-state battery technologies.

6. Microstructure–property relationships and toughening mechanisms

The reviewed studies consistently demonstrated that fracture toughness behavior is fundamentally governed by microstructural evolution and defect architecture. Several recurring toughening mechanisms have been repeatedly reported throughout the literature, as summarized in Table 1.

The literature additionally revealed a recurring hardness–toughness trade-off. Highly refined microstructures often produced elevated hardness but reduced crack tolerance, whereas multiphase and growth-dominated architectures generally improved fracture resistance.

The intricate interplay between these microscopic energy-dissipation paths and their macroscopic engineering outcomes is mapped out in Fig. 2. The schematic illustrates how a propagating crack tip is energetically impeded by localized microstructural features, including the tortuosity induced by crack deflection, the restraining forces of

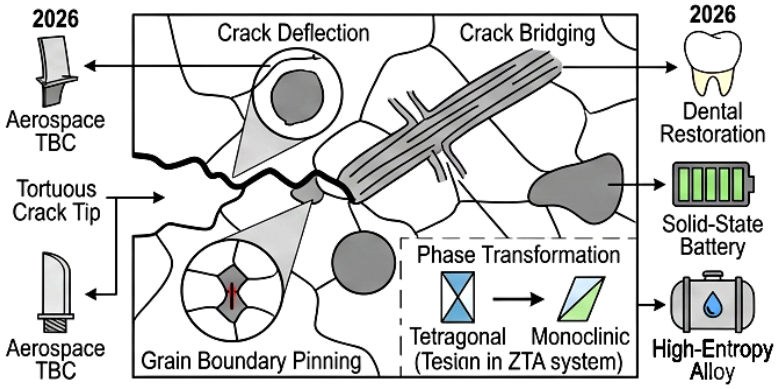

Fig. 2. Microstructure–property relationships and toughening mechanisms.

Table 2. Comparative fracture toughness values of the investigated material systems.

Material system	Fracture toughness ($MPa.m^{1/2}$)
Carbon fiber (C_f)/Si_3N_4 composite	10.87
Al_2O_3/ZrO_2 eutectic composite	up to 9.8
Ti_3AlC_2-derived nanocomposite	7.6
TiB_2-based UHTC	7
TiCrC nanocarbide	6.5
TiO_2–ZTA	6.08
$(TiZrNbTa)C_{0.8}N_{0.2}$ high entropy carbonitride	5.6
ZrB_2–Ti_2AlC composite	5.5
SiC–AlN–VC	5.25
TaB–Si_3N_4	4.40
Nonstoichiometric high-entropy carbide	3.84
HfO_2	3.00
Mullite ceramic	2.9
Additively manufactured ZrC	2.9
Transparent glass-ceramic	2.1
Borotellurite glass	1.764–1.968
RE_3TaO_7	1.0–2.0
SrF_2 transparent ceramic	0.31

crack bridging, grain boundary pinning, and the volumetric expansion associated with tetragonal-to-monoclinic phase transformations in zirconia-toughened systems. By resisting crack opening at the microscale, these mechanisms directly enable the deployment of these advanced ceramics in demanding 2026 applications, ranging from thermal barrier coatings in aerospace systems to high-integrity solid-state batteries and wear-resistant dental restorations.

In general, higher fracture toughness values were associated with microstructural engineering strategies that enhanced resistance to crack initiation and propagation. Fiber reinforcement, multiphase architecture, crack bridging mechanisms, residual stress engineering, SPS-assisted densification, controlled grain growth, and interface strengthening were frequently reported as the primary factors contributing to improved toughness behavior. These mechanisms promoted energy dissipation, crack deflection, and stronger interfacial interactions within the material structure. In contrast, lower fracture toughness values were commonly observed in systems containing high porosity, weak interfacial bonding, brittle monolithic structures, excessive grain coarsening, and amorphous phase accumulation, all of which facilitated crack propagation and reduced structural reliability.

7. Comparative fracture toughness values

The comparative fracture toughness values summarized in Table 2 demonstrate the wide variation in crack resistance among the investigated materials. Carbon fiber/Si_3N_4 and Al_2O_3/ZrO_2 eutectic composites exhibited the highest toughness values, whereas transparent and glass-based materials generally showed lower fracture resistance. Overall, the results indicate that reinforcement mechanisms, microstructural refinement, and multiphase architecture play important roles in improving fracture toughness across advanced ceramic systems.

A visual synthesis of these diverse experimental outcomes is presented in Fig. 3, which categorizes and ranks the reported indentation fracture toughness values from the reviewed 2026 publications. This graphical representation clearly underscores the vast mechanical spectrum covered by the Anstis method, spanning from highly brittle functional systems like SrF_2 transparent ceramics (0.31 $MPa.m^{1/2}$) to exceptional structurally engineered materials such as the carbon fiber/Si_3N_4 composites (10.87 $MPa.m^{1/2}$). The color-coded classification illuminates compositional complexity, particularly in high-entropy carbonitrides and multicomponent ultra-high-temperature ceramics (UHTCs), and consistently shifts the material performance toward higher toughness regimes without completely sacrificing hardness.

8. Emerging trends

Several major research trends emerged from the reviewed 2026 publications. The collected studies demonstrated an increasing emphasis on microstructure-driven fracture toughness optimization through advanced processing and compositional engineering strategies. In addition, growing attention was directed toward multifunctional materials that simultaneously combined improved mechanical performance with thermal, optical, electrical, or biomedical functionalities.

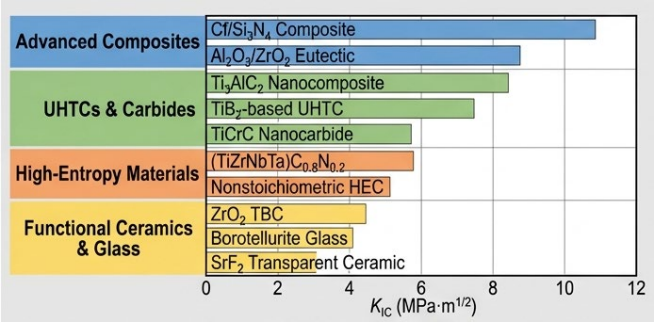

Fig. 3. Comparative fracture toughness values.

8.1. Integration of additive manufacturing

Additive manufacturing approaches, including direct ink writing, digital light processing, and material extrusion, were increasingly integrated with indentation fracture analysis. These techniques enabled the fabrication of complex architectures while maintaining acceptable mechanical performance [5, 6, 35].

8.2. Increasing use of spark plasma sintering

Spark plasma sintering repeatedly appeared across ceramics, carbides, and composites because it enabled enhanced densification and refined microstructures. SPS-assisted processing was employed in Ti_3AlC_2-derived nanocomposites [21], carbon fiber/Si_3N_4 composites [36], $MoSi_2$-MoAlB composites [37], and $B_{12}(C,Si,B)_3$–SiC composites [38].

8.3. Expansion of high-entropy materials

High-entropy alloys, carbides, carbonitrides, and oxide systems represented one of the fastest-growing application areas for the Anstis relationship [15–17].

8.4. Coupling mechanical and functional properties

Many studies simultaneously evaluated fracture toughness together with oxidation resistance, thermal conductivity, ionic conductivity, optical transparency, tribological behavior, hydrogen storage performance, or radiation shielding capability [22, 27, 32, 34].

8.5. Interface engineering and multiscale reinforcement

Interface-controlled toughening mechanisms increasingly emerged as dominant strategies for suppressing brittle fractures. Representative examples included graphene-carbon fiber-reinforced alumina composites [39], Si-doped TiB_2 coatings [40], and SiC-coated carbon/carbon composites [41].

9. Conclusions

The 2026 publications collected demonstrate the continuing importance and applicability of the Anstis relationship in modern materials science research. Although originally developed as an indentation-based fracture toughness estimation method, the relationship now serves as a central characterization framework across ultra-high-temperature ceramics, oxide systems, high-entropy materials, glass-ceramics, thermal barrier coatings, solid electrolytes, transparent ceramics, geological systems, and advanced composites. The reviewed studies collectively reveal that fracture toughness optimization increasingly depends on sophisticated microstructural engineering strategies involving crack deflection, crack bridging, residual stress control, grain refinement, interface tailoring, phase transformation, and multiphase reinforcement. Additive manufacturing, spark plasma sintering, and high-entropy material design have become particularly important in enabling simultaneous improvements in toughness, hardness, thermal stability, oxidation resistance, tribological behavior, and electrochemical performance. The perspective additionally demonstrates that the Anstis relationship remains highly valuable because of its simplicity, broad applicability, and compatibility with modern characterization methods. Across all reviewed systems, fracture toughness evaluation was directly linked to functional reliability in demanding applications ranging from aerospace structures and thermal/environmental barrier coatings to dental restorations, hydrogen storage systems, transparent ceramics, radiation shielding glasses, and all-solid-state batteries. Overall, the reviewed studies illustrate a clear transition from simple indentation-based fracture measurement toward integrated structure–property–performance optimization frameworks in which the Anstis relationship continues to play a foundational role in advanced materials development.

CRediT authorship contribution statement

Maryam Mohammadpour Mokhayer: Writing – original draft, Resources, Methodology.
Mahdiyeh Omrani Khiabanian: Writing – review & editing, Conceptualization, Visualization.

Editorial note

During the peer-review and revision process, and in consultation with the handling editor, the scope of this perspective article was updated to incorporate and discuss relevant literature published during the first months of 2026.

Data availability

No new data were generated in this perspective article.

Declaration of competing interest

The authors declare no competing interests.

Funding and acknowledgment

This research received no external funding.

Declaration of AI-assisted technologies in the writing process

During the preparation of this work, the authors utilized Gemini (an AI collaborator developed by Google) in order to refine the manuscript's structural flow, enhance grammatical clarity, and improve the overall readability of the text. Additionally, the AI tool was employed to conceptualize and generate the structural frameworks for the schematic illustrations presented in this perspective. Following the AI-assisted editing and schematic drafting, the authors reviewed, critically revised, and approved the final contents, and take full responsibility for the scientific integrity, accuracy, and interpretation of the data and conclusions presented in the publication.

References

[1] G.R. Anstis, P. Chantikul, B.R. Lawn, D.B. Marshall, A critical evaluation of indentation techniques for measuring fracture toughness: I, direct crack measurements, J. Am. Ceram. Soc. 64 (1981) 533–538. https://doi.org/10.1111/j.1151-2916.1981.tb10320.x.
[2] C. Li, L. Chen, G. Xue, J. Wang, B. Li, et al., Comprehensive mechanical properties of oxide ceramics measured by nano indentation: RE3TaO7 (RE=La, Sm, Eu, Gd, Dy, Lu) as a study case, Sci. China Mater. 69 (2026) 2178–2187. https://doi.org/10.1007/s40843-025-3779-1.
[3] R. Petráš, R. Kubík, M. Chocholoušek, E.F. Duchková, J. Kekrt, L. Vála, Effect of Pb-16Li long term exposure on mechanical properties

of ceramic materials, Nucl. Mater. Energy. 46 (2026) 102082. https://doi.org/10.1016/j.nme.2026.102082.
[4] A. Koko, A. Abdelnour, T.H. Becker, T.J. Marrow, Bridging experiments and defects' mechanics: a data-driven toolbox for configurational force analysis, Eng. Comput. 42 (2026) 21. https://doi.org/10.1007/s00366-025-02262-5.
[5] F.M. Nogales, A.L. Ortiz, P. Miranda, Direct ink writing and pressureless spark plasma sintering of ultra-high temperature ceramics for the production of complex parts with internal microchannels, J. Eur. Ceram. Soc. 46 (2026) 118236. https://doi.org/10.1016/j.jeurceramsoc.2026.118236.
[6] C. Sabata, Y. Zhou, J.L. Watts, G.E. Hilmas, Thermal and mechanical properties of zirconium carbide manufactured via ceramic on-demand extrusion, J. Eur. Ceram. Soc. 46 (2026) 118159. https://doi.org/10.1016/j.jeurceramsoc.2026.118159.
[7] Z. Ahmadi, M. Farvizi, A. Faraji, M. Bahamirian, P. Amini, M. Shahedi Asl, Ti2AlN MAX phase: An attractive choice for the improvement of mechanical and tribological behavior of ZrB2, Int. J. Refract. Met. Hard Mater. 134 (2026) 107441. https://doi.org/10.1016/j.ijrmhm.2025.107441.
[8] Y. Yu, L. Liu, Y. Zhao, Y. Jin, J. Wei, et al., Fabrication of tantalum monoboride ceramics: Effects of B, SiC, and Si3N 4 additions, J. Am. Ceram. Soc. 109 (2026) e70521. https://doi.org/10.1111/jace.70521.
[9] W. Li, Z. Ma, L. Pan, J. Xu, C. Han, et al., Improving density and properties of spark plasma sintered LaB6 bulk by Ni addition, Ceram. Int. 52 (2026) 11119–11125. https://doi.org/10.1016/j.ceramint.2026.01.276.
[10] W. Li, A. Cheng, H. Liu, S. Fu, W. Ji, Densification mechanism and enhanced properties of fine-grain hafnia ceramics prepared by high-pressure sintering, J. Am. Ceram. Soc. 109 (2026) e70433. https://doi.org/10.1111/jace.70433.
[11] V. Shekhovtsov, Influence of arc plasma parameters and particle size distribution of initial components on structure and properties of synthesized mullite materials, Ceram. Int. 52 (2026) 20570–20585. https://doi.org/10.1016/j.ceramint.2026.03.149.
[12] J. Li, S. Zhai, H. Xu, Y. Wang, Q. Xie, J. Liu, Effects of prolonged heat treatment on the microstructure and mechanical properties of Al2O3/ZrO2(Y2O3) eutectic ceramics, J. Alloys Compd. 1057 (2026) 186846. https://doi.org/10.1016/j.jallcom.2026.186846.
[13] X. Lin, B. Zhang, X. Yan, H. Zhao, B. Li, X. Wang, Influence of TiO2 content on the mechanical properties, wear performance and hydrothermal aging stability in zirconia-toughened alumina composites, Ceram. Int. 52 (2026) 26003–26012. https://doi.org/10.1016/j.ceramint.2026.04.072.
[14] S.K. Paul, A. Rahaman, Role of Nano-Zirconia on the Mechanical and Fracture Behavior of Alumina-Based Composites Prepared through Slip Casting, Phys. Status Solidi. 223 (2026) e202500810. https://doi.org/10.1002/pssa.202500810.
[15] Q. Li, Y. Li, Y. Wang, H. Liang, X. Li, et al., Boosting the strength and toughness of (TiZrNbTa)C0.8N0.2 carbonitride via high-entropy and high-pressure engineering, Appl. Mater. Today. 48 (2026) 103012. https://doi.org/10.1016/j.apmt.2025.103012.
[16] L. Huang, J. Yin, X. You, Y. Zheng, Z. Guo, et al., Effects of carbon stoichiometry on the mechanical and tribological properties of high-entropy (TaNbZrTiMo)C carbide ceramics, Ceram. Int. 52 (2026) 22271–22284. https://doi.org/10.1016/j.ceramint.2026.03.293.
[17] M. Mazloomi, H. Shahmir, F. Forghani, M. Ismail, High-throughput calculations to develop high-entropy alloys for hydrogen storage applications, Int. J. Hydrogen Energy. 228 (2026) 154398. https://doi.org/10.1016/j.ijhydene.2026.154398.
[18] M. Mhadhbi, Microstructural and mechanical properties of spark plasma sintered TiCrC nanocarbide for tools application, Nanotechnology. 37 (2026) 015704. https://doi.org/10.1088/1361-6528/ae2bf5.
[19] Z. Zhang, N. Li, G. Chang, Z. Zhang, W. Wang, et al., Breaking Hardness−Toughness Trade-Off in Novel (V, Nb)C Carbides via Nanoscale Phase Separation and Local-Chemical-Order Dislocation Network, Rare Met. 45 (2026) e70006. https://doi.org/10.1002/rar2.70006.
[20] L. Li, M. Gong, H. Zhang, W. Hai, Interface, Mechanical and Thermal Properties of In Situ Generated V(C,N) Solid Solution Reinforced SiC–AlN–VC Multiphase Ceramics, J. Compos. Sci. 10 (2026) 29. https://doi.org/10.3390/jcs10010029.
[21] O. Messer, B. Ratzker, A. Nitsan, Y. Kushnir, N. Maman, et al., Mechanical destabilization enables defect-driven phase transformation in layered MAX phases, Mater. Today. 97 (2026) 103336. https://doi.org/10.1016/j.mattod.2026.103336.
[22] J. Zhu, Y. Sun, C. Fan, P. Ai, C. Li, et al., An enhanced CMAS corrosion and oxidation resistance performance in Hf6Ta2O17/YSZ thermal barrier coatings with limited ion diffusion ability, Appl. Surf. Sci. 726 (2026) 165928. https://doi.org/10.1016/j.apsusc.2026.165928.
[23] Z. Qiu, Q. Liu, S. Dong, X. Linghu, Y. Huang, et al., Proportional optimization and performance evaluation of YbTaO4-Ta2O5 composite coatings for integrated thermal environmental barrier coatings (TEBCs) on SiCf/SiC composites, Appl. Surf. Sci. 729 (2026) 166136. https://doi.org/10.1016/j.apsusc.2026.166136.
[24] K. Lü, W. Ge, S. Duo, H. Zhang, HfTiO4-TiO2 composites as top-coat candidates for thermal/environmental barrier coatings, Ceram. Int. 52 (2026) 13756–13765. https://doi.org/10.1016/j.ceramint.2026.02.017.
[25] L. Li, B. Zou, X. Cao, Y. Zhang, Y. Wang, et al., Microstructure and properties of thick thermal barrier coatings based on Pr6O11 doped ZrO2 on titanium alloy, Surf. Coatings Technol. 523 (2026) 133244. https://doi.org/10.1016/j.surfcoat.2026.133244.
[26] D. Chai, B. Mei, W. Li, Effect of the sintering temperature on the microstructure and optical quality of SrF2 transparent ceramics with large grain size, Ceram. Int. 52 (2026) 18446–18452. https://doi.org/10.1016/j.ceramint.2026.02.407.
[27] X. Zheng, Z. Yan, J. Lu, S. Liu, B. Guan, et al., Transparent Glass-Ceramics With High Hardness and Fracture Toughness, J. Am. Ceram. Soc. 109 (2026) e70562. https://doi.org/10.1111/jace.70562.
[28] H. Yuan, S. Shen, X. Tong, Q. Li, Y. Huang, et al., Ternary modifier engineering (Na2O–K2O–CaO) in lithium disilicate glass-ceramics: Crystallization pathways, microstructure, and mechanical performance, Ceram. Int. 52 (2026) 22492–22502. https://doi.org/10.1016/j.ceramint.2026.03.312.
[29] S. Shen, H. Yuan, X. Tong, Q. Li, J. Wu, et al., Disentangling the Distinct roles of P2O5 and TiO2 in Nucleation-Controlled Crystallization of Lithium Disilicate Glass-Ceramics, J. Alloys Compd. 1062 (2026) 187392. https://doi.org/10.1016/j.jallcom.2026.187392.
[30] A.Z. Juri, R. Belli, G. De Souza, U. Lohbauer, Y. Nakanishi, L. Yin, In-situ nanomechanical responses of zirconia-containing lithium silicate glass-ceramics, J. Mech. Behav. Biomed. Mater. 177 (2026) 107365. https://doi.org/10.1016/j.jmbbm.2026.107365.
[31] E. Sánchez-González, J.D. Ríos, F. Guiberteau, M.A. Berthaume, M. Hoffman, O. Borrero-López, Effect of rotational forces on the durability of dental materials: implications in biology and anthropology, J. R. Soc. Interface. 23 (2026) 20250682. https://doi.org/10.1098/rsif.2025.0682.
[32] M. Fidan, A. Acikgoz, D. Yılmaz, E. Oruç Ulaş, S. İşgör, Structural and Mechanical Properties, Nuclear Shielding and Albedo Parameters of the B2O3-TeO2–Li2O–CuO-Sb2O3 Glass System, Ceram. Int. 52 (2026) 16023–16041. https://doi.org/10.1016/j.ceramint.2026.02.202.
[33] Y. Pavlovskyy, V. Brytan, O. Kuzyk, Y. Skvarok, Y. Kovalchuk, A. Tymkiv, The influence of growing in a hydrogen atmosphere on the micromechanical properties of Cd1-xZnxTe single crystals, Phys. Chem. Solid State. 27 (2025) 69–73. https://doi.org/10.15330/pcss.27.1.69-73.
[34] H. Lee, Y. Seki, A. Okumura, M. Kodama, Thermal diffusivity and conductivity of sulfide and oxide solid electrolytes: Effects of

densification and microstructural evolution, J. Energy Storage. 145 (2026) 119926. https://doi.org/10.1016/j.est.2025.119926.
[35] J. Tanska, K. Bukowska, P. Wiecinski, P. Falkowski, A. Ostrowski, et al., Influence of Ni and Mo organometallic precursors on the fracture toughness of alumina-metal composites manufactured by Digital Light Processing, Ceram. Int. 52 (2026) 13375–13391. https://doi.org/10.1016/j.ceramint.2026.01.473.
[36] S. Hoseinzadeh, M.R.L. Estarki, A. Ghasemi, S. Zahabi, G. Gordani, E.M. Sharifi, Concurrent optimization of fracture toughness, thermal conductivity, and tribological behavior in Cf/Si3N4 composites via phase driven selection, Sci. Rep. 16 (2026) 10739. https://doi.org/10.1038/s41598-026-44244-7.
[37] X.-A. Bei, G.-H. Zhang, Microstructures and High-Temperature Oxidation Behavior of MoSi2-MoAlB Composites, Corros. Sci. 261 (2026) 113639. https://doi.org/10.1016/j.corsci.2026.113639.
[38] A. Fernández-Ortiz, V. Zamora, F. Guiberteau, A.L. Ortiz, Unlubricated fretting wear of a hard B12(C,Si,B)3–SiC composite reactively sintered from B4C with Si aids, Int. J. Refract. Met. Hard Mater. 138 (2026) 107707. https://doi.org/10.1016/j.ijrmhm.2026.107707.
[39] Y. Zheng, J. Sun, X. Li, L. Zhao, S. Ning, J. Zhao, Three-dimensional graphene-carbon fiber network and dual-phase high-entropy alloy for boosting mechanical responses of alumina ceramics, Adv. Compos. Hybrid Mater. 9 (2026) 155. https://doi.org/10.1007/s42114-026-01743-5.
[40] L. Xian, L. Li, H. Fan, H. Zhao, Z. Yu, J. Zhang, et al., Enhanced Adhesive Wear Resistance of TiB2 Coating Sliding Against Titanium Alloy Grinding Balls by Low-Concentration Si Doping, Vacuum. 246 (2026) 115032. https://doi.org/10.1016/j.vacuum.2025.115032.
[41] C. Tan, J. Hou, R. Wang, Y. Zeng, T. Liu, et al., Prepress-assisted controllable preparation of SiC coating: A novel route to enhanced dynamic oxidation resistance, Ceram. Int. 52 (2026) 10255–10265. https://doi.org/10.1016/j.ceramint.2026.01.201.